EUROPEAN ORGANIZATION FOR NUCLEAR RESEARCH

CERN-EP/82-104
16 July 1982

TRANSVERSE ENERGY CARRIED BY CHARGED PARTICLES IN $\bar{p}p$ AND pp COLLISIONS AT THE CERN INTERSECTING STORAGE RINGS

The Axial Field Spectrometer Collaboration

(Brookhaven[1] - CERN[2] - Copenhagen[3] - Lund[4] - Pennsylvania[5] - RAL[6] - Tel-Aviv[7])

T. Åkesson[4], M.G. Albrow[6], S. Almehed[4], R. Batley[2], O. Benary[7], H. Bøggild[3], O. Botner[2], H. Brody[5], V. Burkert[2], A. Di Ciaccio[1], D. Cockerill[6], S. Dagan[7], E. Dahl-Jensen[3], I. Dahl-Jensen[3], G. Damgaard[3], C.W. Fabjan[2], S. Frankel[5], W. Frati[5], H. Gordon[1], A. Hallgren[2], K.H. Hansen[3], B. Heck[2], H.J. Hilke[2], J.E. Hooper[3], G. Jarlskog[4], P. Jeffreys[6], T. Jensen[2], G. Kesseler[2], T. Killian[1], D. Lissauer[7], B. Lörstad[4], T. Ludlam[1], N.A. McCubbin[6], A. Melin[4], U. Mjörnmark[4], R. Møller[3], W. Molzon[5], B.S. Nielsen[2], A. Nilsson[4], L.H. Olsen[2], Y. Oren[7], L. Rosselet[2], E. Rosso[2], R.H. Schindler[2], B. Schistad[3], E. Vella[5], W.J. Willis[2], M. Winik[1], W. Witzeling[2] and C. Woody[1]

ABSTRACT

Global features of $\bar{p}p$ and pp collisions at a c.m.s. energy of 53 GeV are compared as functions of the summed transverse energy $\sum_c E_T$ of charged particles in the central region $|y| < 0.8$. They are found to be very similar for $\sum_c E_T$ up to $\simeq$ 12 GeV. For both types of collisions, all gross features for $\sum_c E_T$ up to 6-8 GeV are well described by a model that folds together the inclusive multiplicity and p_T distributions. At higher values of $\sum_c E_T$ the data deviate increasingly from the model.

(Submitted to Nuclear Physics B)

---

[1] Brookhaven National Laboratory, Upton, USA.
[2] CERN, Geneva, Switzerland.
[3] Niels Bohr Institute, Copenhagen, Denmark.
[4] University of Lund, Sweden.
[5] University of Pennsylvania, Philadelphia, USA.
[6] Rutherford Appleton Laboratory, Didcot, UK.
[7] University of Tel-Aviv, Israel.

1. INTRODUCTION

When characterizing broad features of inelastic hadron-hadron collisions it is natural to consider a suitably chosen measure of the inelasticity of the collision as a basic parameter. Following Ochs and Stodolsky [1], a quantity often used for this purpose is the total transverse energy $\sum E_T$ emitted into a given range of the scattering angle in the central region. A $\sum E_T$ trigger obviously does not in itself impose any structure on the azimuthal distribution of particles, and in particular does not require that the particles be concentrated in some limited regions of azimuth and rapidity (jets). On the other hand, it was expected that events containing such jets would be dominant at large $\sum E_T$. However, this expectation has recently been found to be in disagreement with both experimental and more refined theoretical results [2,3], at least at SPS/FNAL energies.

Results on the distribution of summed transverse energy $\sum E_T$ over the complete azimuthal range in a part of the central region have been reported by the NA5 group at the CERN SPS (p_{lab} = 300 GeV/c) [2] for $\sum E_T$ up to 18 GeV, and recently from the UA1 group at the SPS collider [4], and from experiment E557 at Fermilab [5]. The cross-section measured by the NA5 group was much larger than predicted from a QCD-inspired model in which events at high $\sum E_T$ were assumed to be dominated by hard constituent scattering. The event structure showed no sign of a major contribution from high-p_T jets.

Here we want to report results from an investigation of inelastic proton-proton and antiproton-proton collisions in the CERN ISR. For this analysis only charged particles are used, and the summed transverse energy $\sum_c E_T$ is formed from tracks observed in the c.m.s. rapidity range $|y| < 0.8$ in a cylindrical drift chamber covering almost 2π in azimuth.

In a previous paper [6], we have compared $p\bar{p}$ and pp interactions in the central region at low p_T. The present paper extends those measurements to higher p_T of the particles. Various characteristics of the events, such as the mean transverse momentum $\langle p_T \rangle$, the mean charged multiplicity $\langle n \rangle$, and the event shape in the transverse plane, are studied as functions of $\sum_c E_T$.

2. APPARATUS AND DATA ANALYSIS

The experiment was performed with the Axial Field Spectrometer (AFS) at the CERN Intersecting Storage Rings (ISR). For the present investigation only the cylindrical drift chamber, shown in fig. 1, and scintillator hodoscopes were used. The coordinate system used is indicated on the figure.

The drift chamber and its performance is described in detail elsewhere [7,8]. It is 1.4 m long, and extends radially from 0.20 to 0.80 m. It is segmented azimuthally in 4° sectors, each with 42 resistive sense wires, which provide the coordinates in the transverse plane from drift time and the position along the sense wire from a measurement of the pulse heights recorded at both ends. It is situated in an axially symmetric magnetic field of ~ 0.5 T. A cylindrical scintillator hodoscope is placed between the vacuum chamber and the drift chamber. It consists of 44 strips, each covering 8° in azimuth and 60 cm long.

The resolution in the drift chamber is 230 μm (r.m.s.) in the drift distance, and 1.5 cm (r.m.s.) in the axial coordinate z. The resulting momentum resolution for full-length tracks is found to be $\Delta p/p \approx \sqrt{(0.025\ p)^2 + (0.01)^2}$ (p in GeV/c), where the first term comes from measurement errors, and the second from multiple scattering in the chamber gas and wires.

The data analysed here were recorded during four ISR runs with $\bar{p}p$ in April and October 1981, and four runs with pp at low luminosity, close in time to the $\bar{p}p$ runs. For one quarter of the $\bar{p}p$ and half of the pp data the field of the magnet was reversed to minimize systematic effects. All data are at a c.m.s. energy of $\sqrt{s} = 53$ GeV.

Two sets of scintillators were placed around the downstream beam pipes to record the luminosity and for use in the trigger. The range of scattering angles covered by these counters was $1.2° < \theta < 6°$.

The trigger used was defined by a coincidence between these downstream beam counters ("beam-beam"), as it was found that including events triggered only by a hit in the central hodoscope resulted in an unacceptably large background in the $\bar{p}p$ runs. Diffractive events are essentially excluded by this trigger.

The cross-section detected by the beam-beam coincidence trigger was $\sim$ 21.0 mb for both the pp and the $\bar{p}p$ runs. The requirement of a beam-beam coincidence may affect the shape of the $\sum E_T$ spectrum if, for example, events with large $\sum E_T$ in the central region have a lower forward multiplicity. We shall ignore this possible correlation, but note that all distributions shown are for events with at least one charged particle with $1.2^\circ < \theta < 6^\circ$ to each beam axis.

Samples of $\sim$ 56,000 $\bar{p}p$ events and $\sim$ 49,000 pp events were fully analysed using the pattern recognition and geometry programs [9] developed for the AFS. To increase statistics at high $\sum_c E_T$, a fast software filter was devised that selected events with a large $\sum_c E_T$ based on the raw digitizings in the outer 2/3 of the drift chamber. Samples of $\sim$ 180,000 raw events of each type were processed with this filter program, which accepted $\sim$ 9% of them for full analysis. The frequency and structure of these selected events were found to be consistent with those from the fully analysed samples for $\sum_c E_T > 4$ GeV in the region of phase space considered (see below), and the samples have been combined where appropriate above this transverse energy.

Events were accepted for the analysis if they either had a vertex in an appropriate fiducial box around the centre of the interaction diamond or at least one accepted track passing this box, and if in any case they had at least one accepted track (according to criteria described below). Events that were accepted without having a reconstructed primary vertex had a very low multiplicity of accepted tracks, $\sim$ 90% being 1-prong events.

The cuts imposed on the tracks were chosen to ensure that accepted tracks passed close to a reconstructed primary vertex or to the centre of the interaction diamond, and that the momentum-measurement error was small [$\Delta p/p < 0.06$ for $p < 2$ GeV/c, $\Delta(1/p) < 0.03$ GeV^{-1} for $p > 2$ GeV/c].

All accepted tracks were transformed to the c.m.s., and their c.m.s. rapidity and transverse energy were calculated using a pion mass. The acceptance was found to be nearly uniform in rapidity for $|y| < 0.8$ and uniform in azimuth in the regions $|\phi| < 80^\circ$ and $110^\circ < \phi < 250^\circ$, i.e. a total azimuthal range of $\Delta\phi = 300^\circ$.

In this region the acceptance was identical within a few per cent for both charges and both polarities of the magnetic field. For the present analysis, tracks were only accepted in this region of phase space. A few events (6/32000) contained a track with a measured $p_T > 5$ GeV/c, where fewer than one are expected in a sample of this size. They were rejected in the subsequent analysis, as they are almost certainly tracks that simulate a high-p_T track in our chamber, through pattern recognition difficulties, decays in flight, etc. The final samples are summarized in table 1.

The p_T distributions of charged particles in pp and $\bar{p}p$ collisions are shown in fig. 2, normalized to the trigger cross-sections. The p_T distributions are seen to be identical within errors for p_T up to 5 GeV/c. This extends our previous comparison [6], which went only to a p_T of 1.5 GeV/c. From the pp events, and from the $\bar{p}p$ events from the last runs, where background was not severe, we find that 20% of the triggers do not contain an accepted track in the acceptance region.

Also shown in fig. 2 is the inclusive spectrum $(1/\sigma_{in}) \times (d\sigma/dy\, d\, p_T)$ at $y = 0$, measured by the British-Scandinavian Collaboration [10]. The shape, as well as the normalization, is seen to agree well with the present measurements for p_T up to 5 GeV/c. This indicates that the non-diffractive events selected in the present study have a p_T distribution in the region studied similar to the inclusive distribution, and that the acceptance is uniform for $p_T > 0.2$ GeV/c, and is close to 100%.

For $p_T < 0.2$ GeV/c our acceptance is less than 1.0 (~ 0.80 for $0.1 < p_T < 0.2$ GeV/c, and ~ 0.25 for $p_T < 0.1$ GeV/c), as shown by the comparison with the inclusive spectrum, assuming that the agreement between the spectra extends also to this low-p_T region. No corrections have been applied for this inefficiency in the following. The effect on $\sum_c E_T$ is negligible, whereas the correction to the observed multiplicity is estimated to be around 10%. (15% at the lowest values of $\sum_c E_T$.)

For comparison with the data, a model was constructed in which the particles are distributed in multiplicity (fig. 3) and p_T (fig. 2) as the inclusive distributions [10] (with acceptance weights as above for $p_T < 0.2$ GeV/c), and the distributions in rapidity and azimuth are flat in the regions $|y| < 0.8$ and $|\phi| < 80°$ or $110° < \phi < 250°$. The effects of energy-momentum conservation are neglected, as well as particle correlations, apart from those implicit in the multiplicity distribution. The model is not meant to be "as realistic as possible", but is merely to provide a point of reference to the data with the absolute minimum of input. As will be seen, this "model" successfully reproduces both the $\sum_c E_T$ spectrum and various other features of the data at low or moderate $\sum_c E_T$.

The multiplicity distributions observed in the region of acceptance are shown in fig. 3 for pp and $\bar{p}p$ collisions. No significant differences are seen.

Also shown on the figure are two lines representing extreme limits to the high multiplicity tail of the distributions. These are used as limits in the model calculations to indicate the dependence of the results on the multiplicity distribution assumed.

3. TRANSVERSE ENERGY CARRIED BY CHARGED PARTICLES

In fig. 4a the spectra of $\sum_c E_T$ for $\bar{p}p$ and pp collisions are shown for the region $|y| < 0.8$, $\Delta\phi = 300°$, as defined above. They are presented as frequency spectra, i.e. normalized to an area of one. Figure 4b shows the ratio of these distributions as a function of $\sum_c E_T$. The distributions are seen to be remarkably similar for the two types of collisions. They are consistent with being exponential, with a slope of 1.1 GeV^{-1}, for $\sum_c E_T > 2$ GeV.

The main contributions to the systematic error in the energy scale come from the determination of the track acceptance, and from the use of pion masses for all particles. It is estimated to be less than 10%.

The simple model described above reproduces the data well up to $\sum_c E_T \approx 6$ GeV, above which it deviates increasingly for increasing $\sum_c E_T$.

The average transverse energy is observed to be proportional to the multiplicity n of charged particles in the acceptance region, as shown in fig. 5. The average E_T per particle is found to be 0.45 GeV. This value is somewhat higher than the value of $\langle E_T \rangle$ derived from inclusive measurements, because of the loss of particles below p_T = 0.2 GeV/c. The corrected value is 0.39 GeV (assuming a pion mass for all particles). The linear behaviour is, by construction, well described by the model. The average $\sum_c E_T$ for all multiplicities ($\geq$ 1) is 1.44 GeV for the region $|y| < 0.8$, $\Delta\phi = 300°$.

The mean multiplicity is shown as a function of $\sum_c E_T$ in fig. 6a. The observed over-all mean multiplicities in the pp and $\bar{p}p$ samples are 3.27 ± 0.01 and 3.21 ± 0.01, respectively (statistical errors only). These values are consistent with being equal, within an estimated systematic error of a few per cent that originates mainly from the difficulty in establishing correct cuts for the lowest multiplicity events. This small systematic difference in the multiplicities is reflected in the slight deviation from unity (by a few per cent) of the ratio of the $\sum_c E_T$ spectra seen in fig. 4b.

The mean multiplicity at a given $\sum_c E_T$ is the same in $\bar{p}p$ and pp collisions, within errors, and, at the highest $\sum_c E_T$ around 10 GeV, almost 4 times larger than the over-all mean. The tendency for the mean multiplicity to level off at high values of $\sum_c E_T$ is not reproduced by the model calculation, and somewhat larger values of $\langle n \rangle$ than observed are reached in the model at high $\sum_c E_T$.

In fig. 6b the multiplicity distribution is shown in five bins of $\sum_c E_T$. For the sake of clarity, only pp collisions are shown. The distributions have been normalized to the total number of accepted events. One clearly sees that the high multiplicities are mainly obtained from events with a high $\sum_c E_T$.

The mean p_T per particle is shown as a function of $\sum_c E_T$ in fig. 7a. It is found to grow linearly with $\sum_c E_T$, as $\langle p_T \rangle$ = 0.33 GeV + 0.043 $\sum_c E_T$, for both pp and $\bar{p}p$ collisions. Again the model describes the data well at low $\sum_c E_T$ but deviates at $\sum_c E_T$ above 6-8 GeV, where the mean p_T in the model is slightly lower, corresponding to the somewhat elevated multiplicity in the same $\sum_c E_T$ region.

Figure 7b shows the p_T distribution in five bins of $\sum_c E_T$ (for pp collisions only). At low values of $\sum_c E_T$, where the influence of the $\sum_c E_T$ binning is felt, the spectra fall off faster than exponential. In the highest bins of $\sum_c E_T$ a flattening of the spectra at high p_T, relative to an exponential distribution, apparently starts to emerge.

For each event the highest transverse momentum observed is called p_T^{max}. The distribution of p_T^{max} depends rather strongly on $\sum_c E_T$, as can be seen from figs. 8a and b. Figure 8a shows $\langle p_T^{max} \rangle$ as a function of $\sum_c E_T$ for $\bar{p}p$ and pp collisions, and as calculated in the model. The average maximum transverse momentum $\langle p_T^{max} \rangle$ reaches values of about 2.5 GeV/c for values of $\sum_c E_T$ around 10 GeV.

The distribution of p_T^{max} is shown in fig. 8b in bins of $\sum_c E_T$. The lines on the figure are drawn to guide the eye. The slope at large p_T^{max} decreases considerably as $\sum_c E_T$ is increased and the region of low p_T^{max} is suppressed, but simultaneously the width of the distribution increases such that even at the highest values of $\sum_c E_T$ a large fraction of the events have rather modest values of p_T^{max} (e.g. for $\sum_c E_T$ = 8-12 GeV 25% of the events have $p_T^{max} < 1.5$ GeV/c).

From these plots it appears that $\bar{p}p$ and pp collisions are remarkably similar, and that the data up to $\sum_c E_T \approx 6$ GeV are well described by a rather minimal model, which in particular does not have any jet structures built in. At larger values of $\sum_c E_T$ deviations from the model start to emerge. This will receive further attention in the next section.

The spectrum of $\sum_c E_T$ clearly depends on the region of phase space over which the sum is formed. Figure 9a gives the distributions of $\sum_c E_T$ in four rapidity intervals, $|y| < 0.2$, 0.4, 0.6, and 0.8, all with $\Delta\phi = 300°$. For the sake of clarity, only data from pp collisions are shown. The over-all mean multiplicities in the four regions are summarized in table 2, together with the slopes of the $\sum_c E_T$ spectra for $\sum_c E_T > 2$ GeV.

In fig. 9b are shown the $\sum_c E_T$ distributions obtained by keeping the rapidity interval $|y| < 0.8$, but limiting the ϕ interval to $|\phi| < 37.5°$ and $|\phi| < 75°$, thus

simulating calorimeter "jet triggers". The phase-space volumes of these regions are the same as the two first regions above and the lines on fig. 9b are taken from fig. 9a. The distributions agree rather well with the corresponding distributions in "slabs" of y. The small differences in slope may be understood from the fact that the rapidity distribution in the central region is not completely flat.

The variation of $\langle n \rangle$ as a function of $\sum_c E_T$ with the rapidity intervals used is shown in fig. 10. The steeper fall-off of the multiplicity distribution in a smaller solid angle forces $\langle n \rangle$ to level off at a smaller value of $\sum_c E_T$. This in turn implies that the mean p_T at a given (high) $\sum_c E_T$ is larger when the same transverse energy is required in a smaller solid angle.

4. EVENT SHAPE AS A FUNCTION OF $\sum_c E_T$

In this section we turn to an investigation of the shape of the events, on an event-by-event basis. In order to do this in a quantitative way, we introduce a quantity C (excluding one-prong events), which we call the "circularity" of the event:

$$C = 2 \left| \sum q_T^2 \Big/ \sum p_T^2 \right|_{min} . \qquad (1)$$

For a given axis in the transverse plane q_T is the momentum component of the $\vec{p}_T$ of the track perpendicular to this axis. The circularity C can be found by diagonalizing the transverse-momentum tensor, and is the two-dimensional equivalent of the sphericity used in e^+e^- jet analysis. It is related to the "planarity" P, used by the NA5 group [2] and others, by $C = 1 - P$. An isotropic, high-multiplicity event would have $C = 1$, and an event consisting of pencil-like jets, collinear in the transverse plane, would have $C = 0$.

Figure 11 shows the distribution of C in pp and $\bar{p}p$ collisions in four bins of $\sum_c E_T$. Results of the model calculation are also shown. The distributions are similar in pp and $\bar{p}p$ collisions, with only small deviations from the model results. The average values of C, shown in fig. 12 as functions of $\sum_c E_T$, are also

very similar in pp and $\bar{p}p$ collisions. For values of $\sum_c E_T$ above 6-8 GeV, the model calculation clearly gives values of $\langle C \rangle$ above those seen in the data, however. From these distributions one can conclude that the high $\sum_c E_T$ events in the present $\bar{p}p$ and pp samples are not dominated by high-p_T two-jet events.

It appears from these considerations that the requirement of large $\sum_c E_T$ is not a very efficient way to select high-p_T jet events at least up to $\sim$ 8 GeV per unit of y. Whether this is still true when much higher values of $\sum_c E_T$ are reached at ISR energies is not known at present, but should be answered soon, when data using the calorimeter of the AFS [8] become available. It does not appear to be the case at lower energies [2].

Fox and Kelly [3] have calculated the $\sum E_T$ spectrum at SPS energies using a QCD-based model that includes gluon bremsstrahlung. In their model, events with a high $\sum E_T$ are mainly events with much bremsstrahlung, and the results indicate that a $\sum E_T$ trigger may emphasize the hadronization processes that form part of the evolution of a high-p_T scattering. Including hadronization effects brings their calculations into good agreement with the measurements of the NA5 group [11].

The evolution of event shapes with $\sum_c E_T$, in events triggered by a single high-p_T particle, is treated elsewhere [12].

5. CONCLUSIONS

The inclusive p_T distribution of charged particles in the central rapidity range $|y| < 0.8$ in pp and $\bar{p}p$ collisions at $\sqrt{s}$ = 53 GeV are found to be similar up to $p_T \approx 5$ GeV/c.

The spectra of transverse energy $\sum_c E_T$ in the phase-space region $|y| < 0.8$, $\Delta\phi = 300°$, are likewise similar in the two types of collisions up to $\sum_c E_T \approx 12$ GeV. Various aspects of the event structure -- $\langle n \rangle$, $\langle p_T \rangle$, and $\langle p_T^{max} \rangle$ as functions of $\sum_c E_T$, the distributions of p_T and p_T^{max}, and the event shape in the transverse plane, characterized by the distribution of circularity -- have also been compared as functions of $\sum_c E_T$, and found to be similar.

As $\sum_c E_T$ is increased, not only does the multiplicity increase strongly but the $\langle p_T \rangle$ per particle increases, reaching $\sim$ 750 MeV/c, with $\sim$ 10 particles per unit y at $\sum_c E_T \sim 10$ GeV.

All of these features are well described at moderate values of $\sum_c E_T$ by a simple model with the distributions of p_T and multiplicity taken from the data, with flat y and ϕ distributions in the acceptance region, and with no built-in correlations. For $\sum_c E_T > 6$-8 GeV some deviations from the model are seen, in the direction expected from the presence of high-p_T jets, i.e. less multiplicity, higher $\langle p_T \rangle$ and smaller circularity. Before drawing further conclusions the data should be compared with a more realistic model. A modification of the model including momentum conservation in the transverse plane, ρ production and p_T-independent rapidity correlations does not appear to improve the agreement with the data at large $\sum_c E_T$. However, in the range investigated here, large $\sum_c E_T$ events seem to be dominated by high multiplicity, with no strong contribution from simple high-p_T jet production.

Acknowledgements

We acknowledge with thanks the work of the CERN Experimental Facilities Division on the drift-chamber construction, and that of the Experimental Support Group of the ISR Division, who installed the experiment. Without the fine achievements of the CERN PS and ISR Divisions and the Antiproton Accumulator Group the work with antiprotons could not have been done. We thank P. Dam, W.M. Evans, P. Frandsen, M.D. Gibson, J.W. Hiddleston, H. Hofmann, J. v.d. Lans, J. Lindsay, E. Lohse, and A. Rudge for their contributions to the experiment. Support from the Research Councils in our home countries is gratefully acknowledged.

REFERENCES

[1] W. Ochs and L. Stodolsky, Phys. Lett. 69B (1977) 225.
W. Ochs, Physica Scripta 19 (1979) 127.

[2] C. De Marzo et al., Phys. Lett. 112B (1982) 173.

[3] G.C. Fox and R.L. Kelly, preprint LBL-13985, submitted to Second Topical Forward Collider Physics Conference, Madison, Wisconsin, Dec. 1981.

[4] G. Arnison et al., Phys. Lett. 107B (1981) 320.

[5] B. Brown et al., Fermilab-Conf.-82/34 EXP, presented by C. Halliwell at 17th Rencontre de Moriond, Les Arcs, March 1982.

[6] T. Åkesson et al., Phys. Lett. 108B (1982) 58.

[7] D. Cockerill et al., Nucl. Instrum. Methods 176 (1980) 159.

[8] H. Gordon et al., Nucl. Instrum. Methods 196 (1982) 303.
O. Botner et al., Nucl. Instrum. Methods 196 (1982) 315.

[9] S. Almehed and B. Lörstad, Comput. Phys. Commun. 22 (1981) 209.

[10] B. Alper et al., Nucl. Phys. B100 (1975) 237.

[11] R.D. Field, contribution to 13th Int. Symposium on Multiparticle Dynamics, Volendam, June 1982.

[12] T. Åkesson et al., contribution to 21st Int. Conf. on High-Energy Physics, Paris, 1982.

Table 1

Final data samples after cuts.
All samples are at $\sqrt{s}$ = 53 GeV.

	Accepted events (Beam-beam trigger with ≥ 1 track)	Accepted events (Filtered data)	Equivalent number of unfiltered events
pp	31,512	15,385	130,000
$\bar{p}p$	33,085	12,613	117,000

Table 2

$\langle n \rangle$ and slope (GeV^{-1}) of the $\sum_c E_T$ distribution for $\Delta\phi = 300°$ in four y intervals, $|y| < y_0$, for pp collisions at $\sqrt{s}$ = 53 GeV. The average multiplicities are for $n \geq 1$. Errors are statistical only.

y_0	0.2	0.4	0.6	0.8
$\langle n \rangle$	1.552 ± 0.006	2.161 ± 0.008	2.754 ± 0.010	3.270 ± 0.011
slope	-2.14 ± 0.10	-1.50 ± 0.05	-1.30 ± 0.05	-1.12 ± 0.05

Figure captions

Fig. 1 : a) Schematic drawing of the Axial Field Magnet and the vertex drift chamber.

b) End view of the drift chamber.

c) Expanded view of a sector structure. The staggering of the sense wires, shown as crosses, has been exaggerated by a factor of five.

Fig. 2 : Observed p_T distributions for charged particles in pp and $\bar{p}p$ collisions at 53 GeV. The solid line shows the inclusive spectrum $(1/\sigma_{in})/(d\sigma/dy\, d\, p_T)$ [10], at $y = 0$.

Fig. 3 : Observed multiplicity distributions of charged particles in pp and $\bar{p}p$ collisions at 53 GeV, in the region $|y| < 0.8$, $\Delta\phi = 300°$. No corrections have been made for the partial loss of particles with $p_T < 0.2$ GeV/c. The lines show extreme representations of the frequencies at high multiplicities used in a model calculation described in the text.

Fig. 4a : Spectrum of $\sum_c E_T$ in the region $|y| < 0.8$, $\Delta\phi = 300°$, for pp and $\bar{p}p$ collisions at $\sqrt{s} = 53$ GeV. The data are normalized to the number of accepted events (see text). Also shown are the results of a simple model calculation discussed in the text.

Fig. 4b : Ratio between the $\sum_c E_T$ spectra in $\bar{p}p$ and pp collisions at 53 GeV, as a function of $\sum_c E_T$.

Fig. 5 : $\langle \sum_c E_T \rangle$ as a function of the multiplicity n of charged particles in the region $|y| < 0.8$, $\Delta\phi = 300°$. Also shown are the model results.

Fig. 6a : Average multiplicity $\langle n \rangle$ of charged particles in the region $|y| < 0.8$, $\Delta\phi = 300°$, as a function of $\sum_c E_T$, for $\bar{p}p$ and pp collisions at 53 GeV. Also shown are the model results. No corrections have been applied for the partial loss of particles with $p_T < 0.2$ GeV/c.

Fig. 6b : Multiplicity distribution of charged particles in pp collisions at 53 GeV in the region $|y| < 0.8$, $\Delta\phi = 300°$, in bins of $\sum_c E_T$. The distributions have been normalized to the total number of events.

Fig. 7a : $\langle p_T \rangle$ as a function of $\sum_c E_T$ for $\bar{p}p$ and pp collisions at 53 GeV. Also shown are the model results described in the text. No corrections have been applied for the partial loss of particles with $p_T < 0.2$ GeV/c.

Fig. 7b : The p_T distribution of charged particles in pp collisions at 53 GeV in the region $|y| < 0.8$, in bins of $\sum_c E_T$. The distributions have been normalized to the number of events in each $\sum_c E_T$ bin.

Fig. 8a : $\langle p_T^{max} \rangle$ as a function of $\sum_c E_T$ for $\bar{p}p$ and pp collisions at 53 GeV, in the region $|y| < 0.8$, $\Delta\phi = 300°$. Also shown are the model results described in the text.

Fig. 8b : Distribution of p_T^{max} among the charged particles in pp collisions at 53 GeV in the region $|y| < 0.8$, $\Delta\phi = 300°$, in bins of $\sum_c E_T$. The distributions have been normalized to the number of events in each $\sum_c E_T$ bin.

Fig. 9a : Distribution of $\sum_c E_T$ in pp collisions at $\sqrt{s} = 53$ GeV, for four rapidity intervals, $|y| < 0.2$, 0.4, 0.6, and 0.8, with $\Delta\phi = 300°$.

Fig. 9b : Distribution of $\sum_c E_T$ in pp collisions at $\sqrt{s} = 53$ GeV, for two intervals of azimuth, $\Delta\phi = 75°$ and $\Delta\phi = 150°$, with $|y| < 0.8$.

Fig. 10 : $\langle n \rangle$ as a function of $\sum_c E_T$ in pp collisions at $\sqrt{s} = 53$ GeV, for four rapidity intervals, $|y| < 0.2$, 0.4, 0.6, and 0.8, with $\Delta\phi = 300°$.

Fig. 11 : a-d Distribution of circularity C in pp and $\bar{p}p$ collisions, in four bins of $\sum_c E_T$. Also shown are the results of the model calculation described in the text.

Fig. 12 : Mean circularity as a function of $\sum_c E_T$ for pp and $\bar{p}p$ collisions, and as calculated in the model.

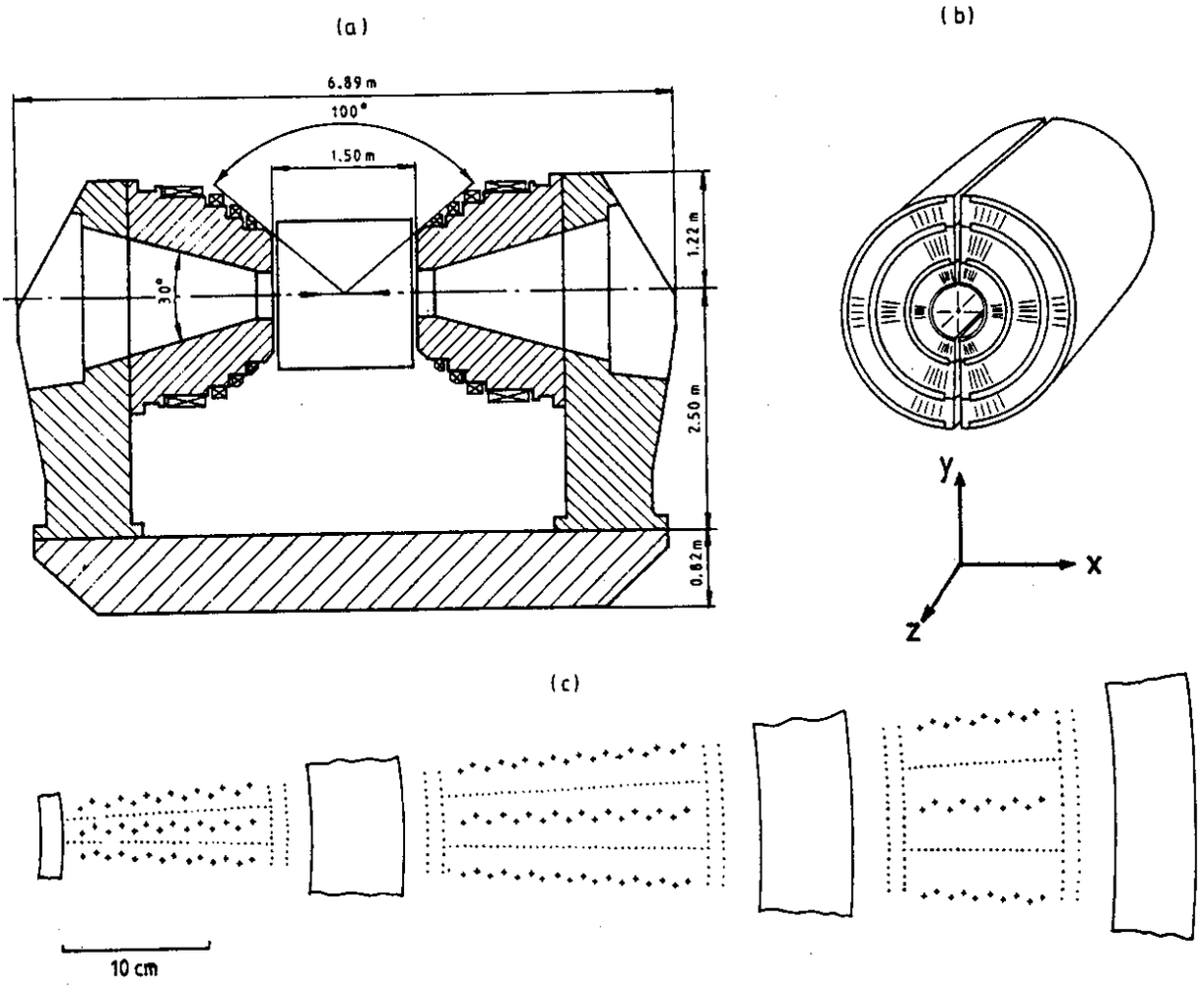

Fig. 1

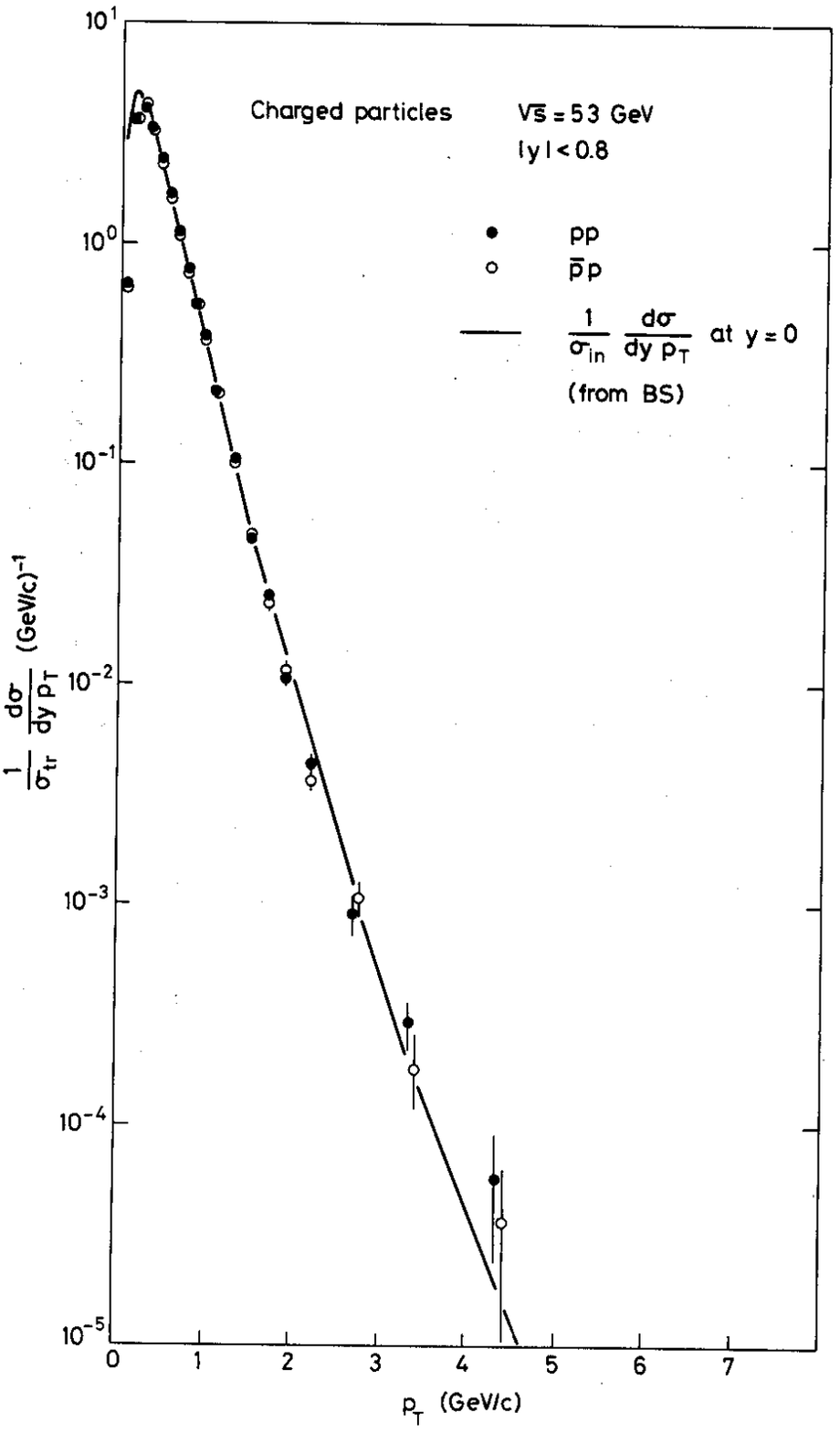
Charged particles
√s = 53 GeV
|y| < 0.8
pp
p̄p
1/σ_in dσ/dy p_T at y = 0
(from BS)
1/σ_tr dσ/dy p_T (GeV/c)^-1
p_T (GeV/c)
10^1
10^0
10^-1
10^-2
10^-3
10^-4
10^-5
0
1
2
3
4
5
6
7

Fig. 2

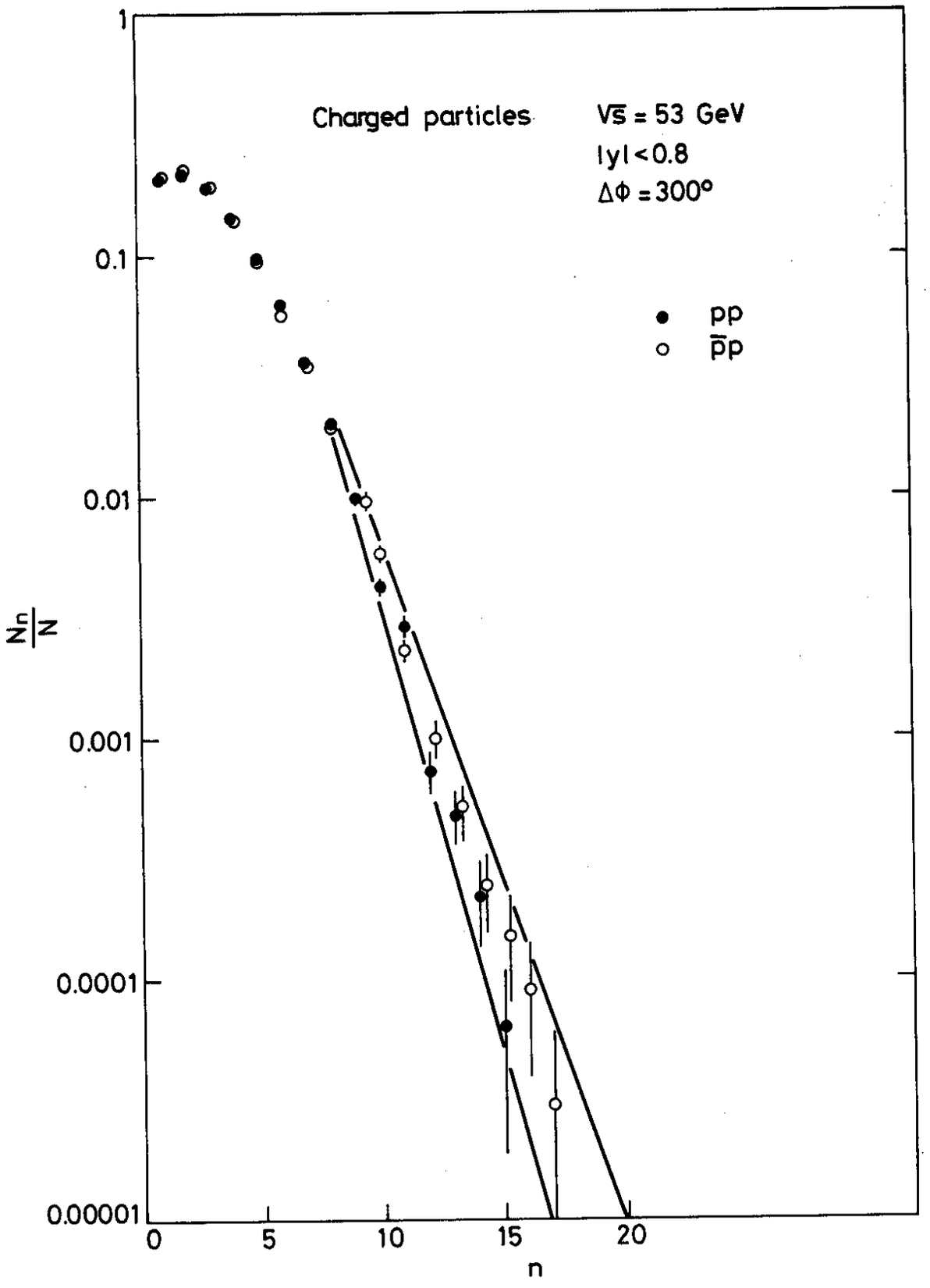
Charged particles
√s = 53 GeV
|y| < 0.8
Δφ = 300°
pp
p̄p
1
0.1
0.01
0.001
0.0001
0.00001
Nn/N
0
5
10
15
20
n

Fig. 3

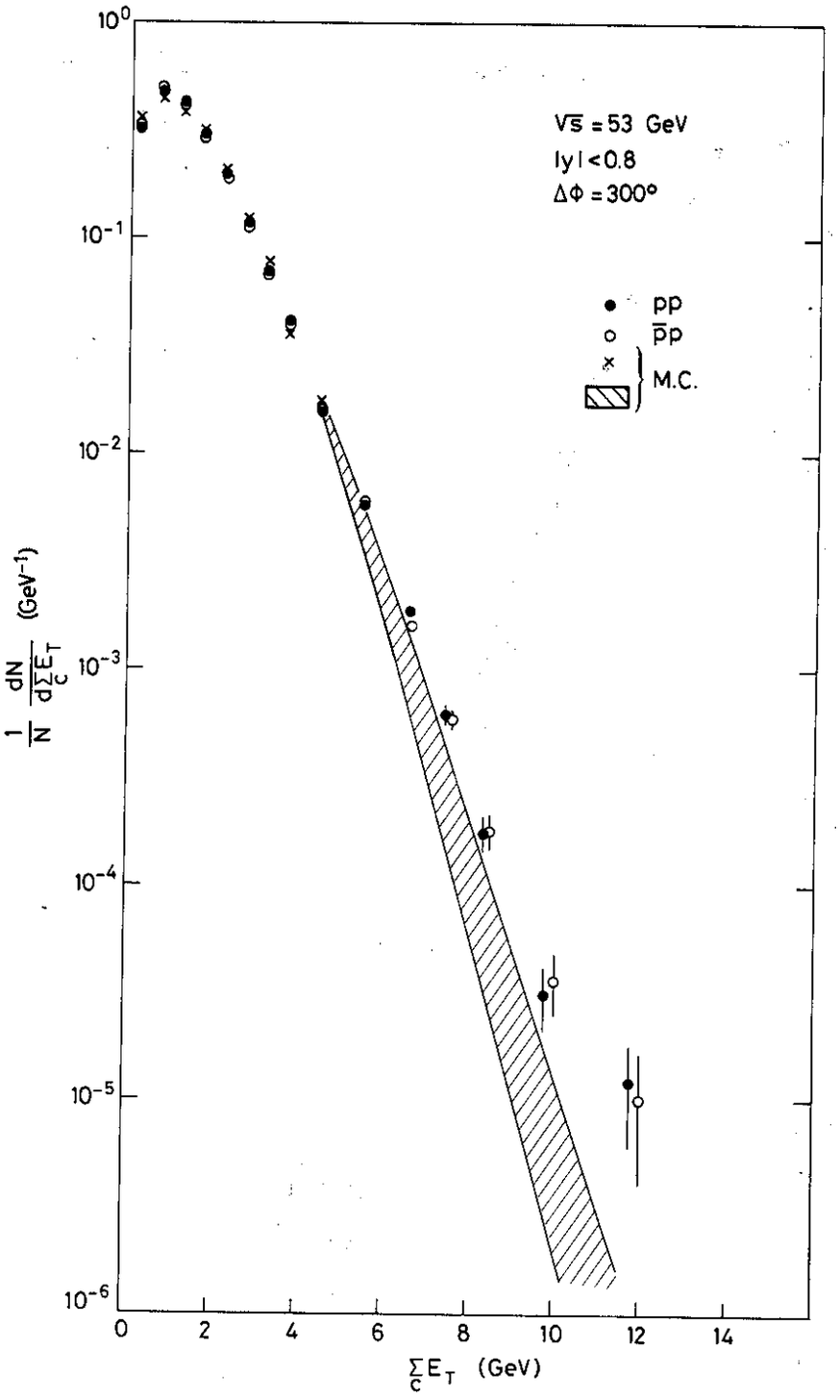
10^0
10^{-1}
10^{-2}
10^{-3}
10^{-4}
10^{-5}
10^{-6}
$\frac{1}{N}\frac{dN}{d\sum_c E_T}$ (GeV^{-1})
$\sqrt{s}$ = 53 GeV
|y| < 0.8
$\Delta\Phi$ = 300°
pp
$\bar{p}p$
M.C.
0
2
4
6
8
10
12
14
$\sum_c E_T$ (GeV)

Fig. 4 a)

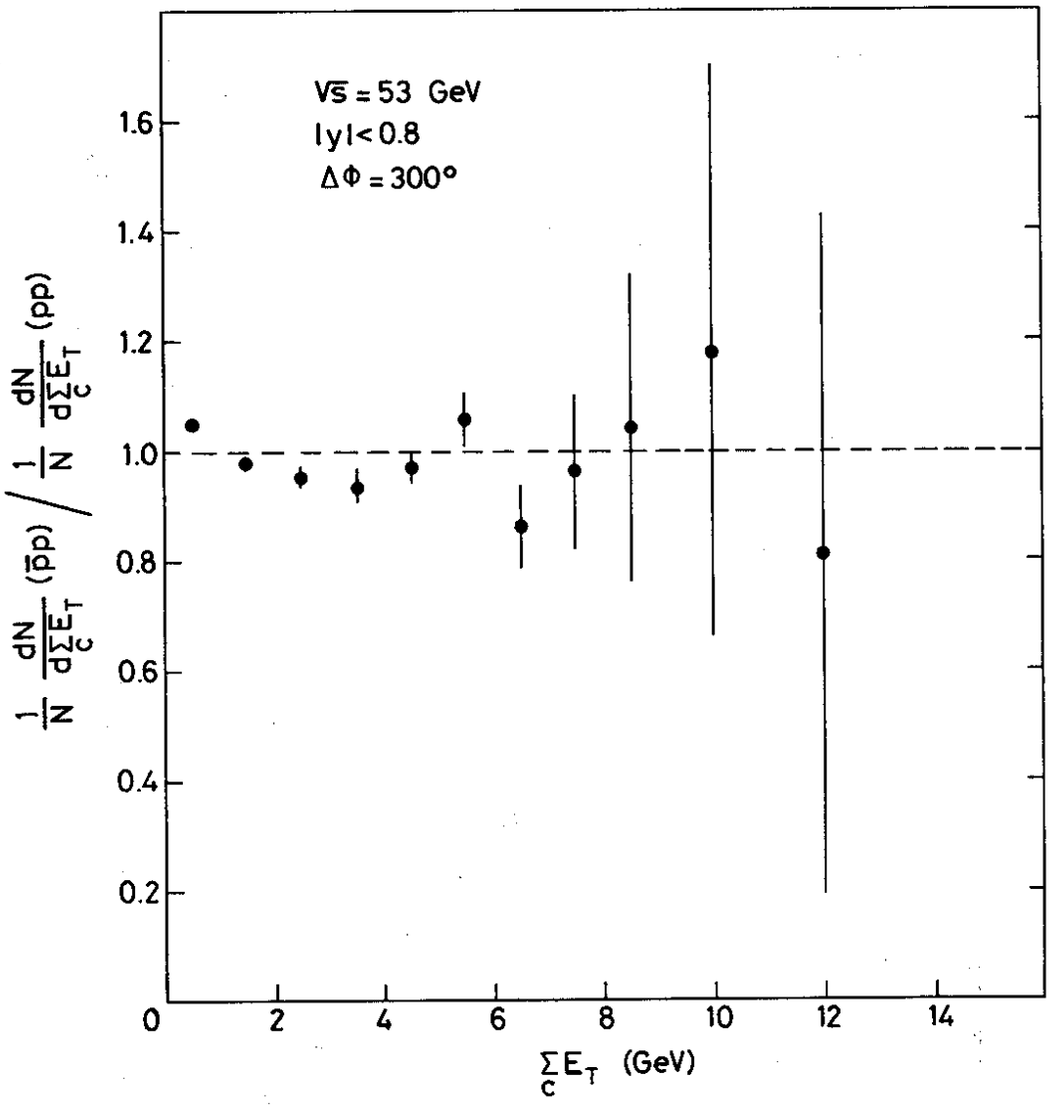
√s = 53 GeV
|y|< 0.8
Δ Φ = 300°
1.6
1.4
1.2
1.0
0.8
0.6
0.4
0.2
0
2
4
6
8
10
12
14
$\frac{1}{N}\frac{dN}{d\sum_c E_T}(\bar{p}p) \Big/ \frac{1}{N}\frac{dN}{d\sum_c E_T}(pp)$
$\sum_c E_T$ (GeV)

Fig. 4 b)

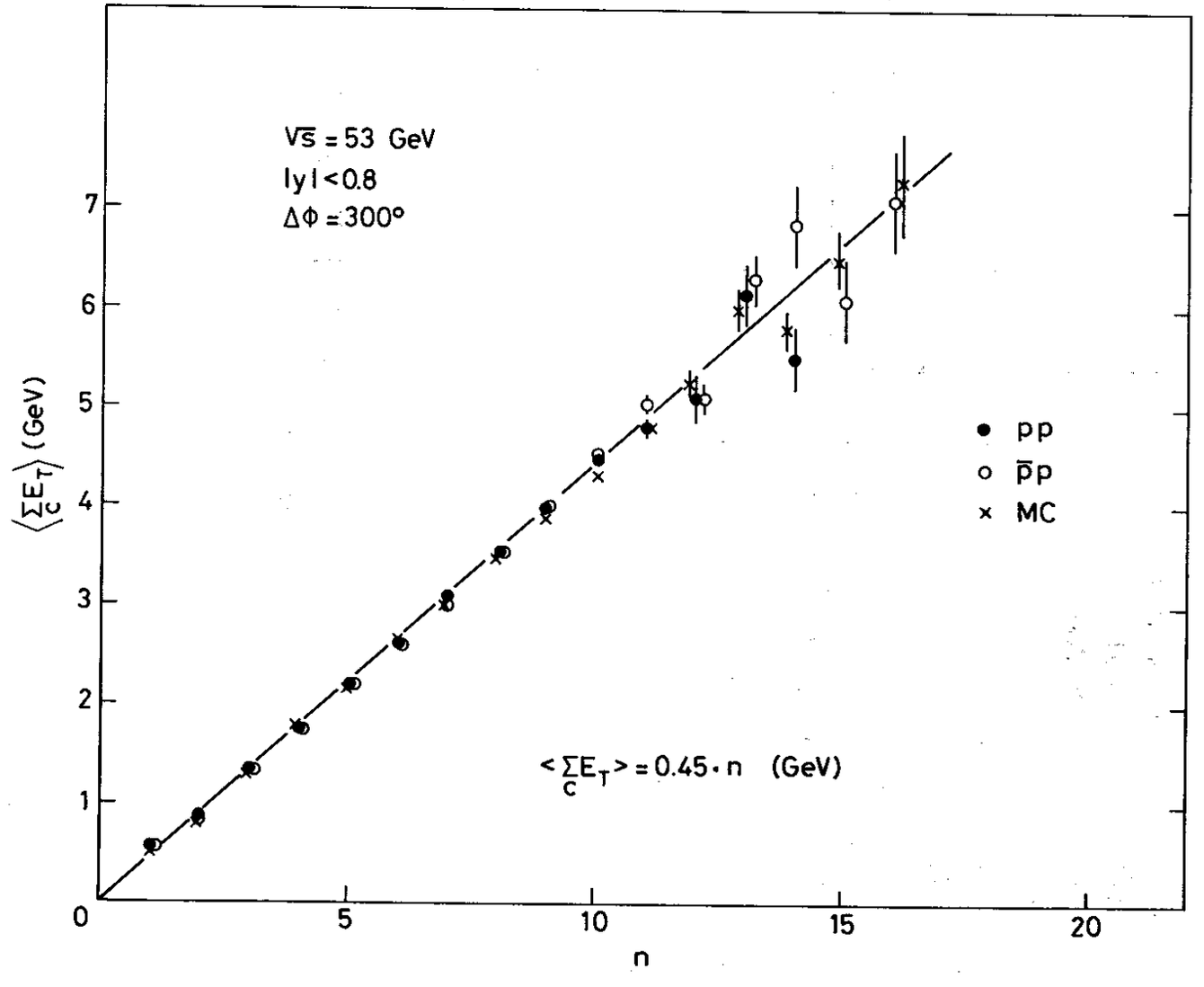
√s = 53 GeV
|y| < 0.8
Δφ = 300°
pp
p̄p
MC
$\langle \sum_c E_T \rangle$ (GeV)
$\langle \sum_c E_T \rangle = 0.45 \cdot n$ (GeV)
n
0
1
2
3
4
5
6
7
5
10
15
20

Fig. 5

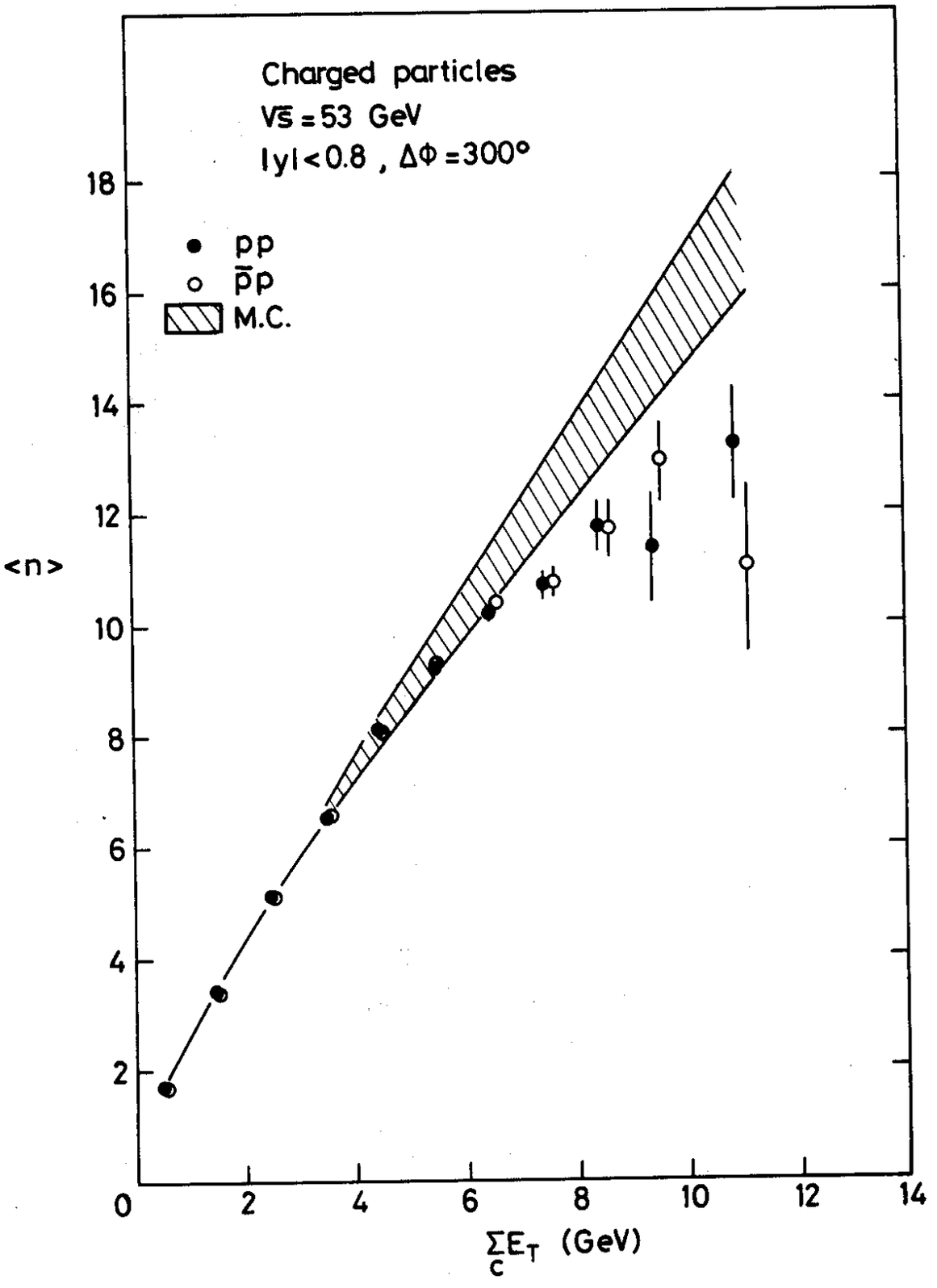
Charged particles
√s = 53 GeV
|y| < 0.8 , Δφ = 300°
pp
p̄p
M.C.
<n>
ΣE_T (GeV)
0
2
4
6
8
10
12
14
16
18

Fig. 6 a)

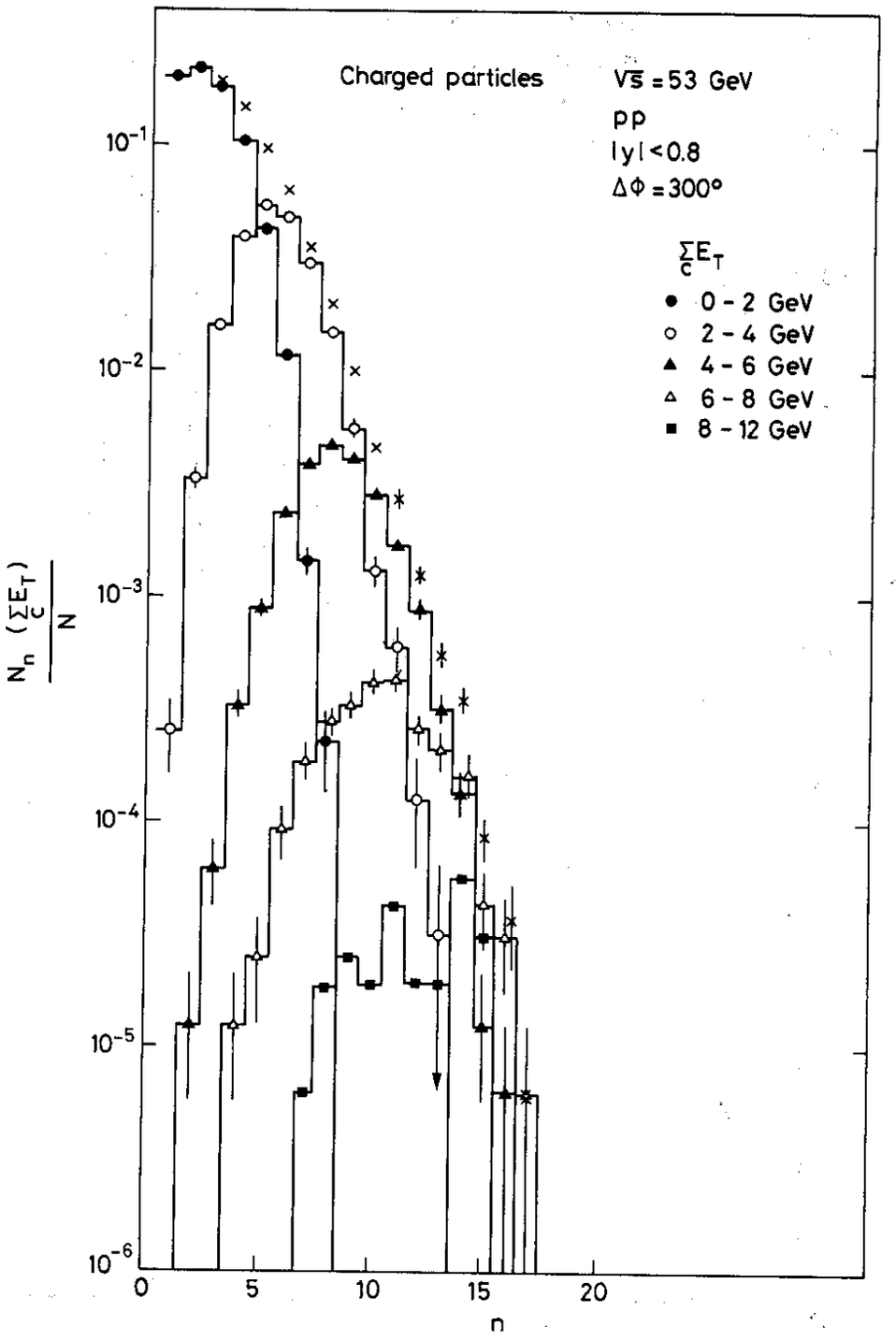
Charged particles
$\sqrt{s}$ = 53 GeV
pp
|y| < 0.8
Δφ = 300°
$\sum_c E_T$
0 - 2 GeV
2 - 4 GeV
4 - 6 GeV
6 - 8 GeV
8 - 12 GeV
$\frac{N_n\ (\sum_c E_T)}{N}$
10^{-1}
10^{-2}
10^{-3}
10^{-4}
10^{-5}
10^{-6}
0
5
10
15
20
n

Fig. 6 b)

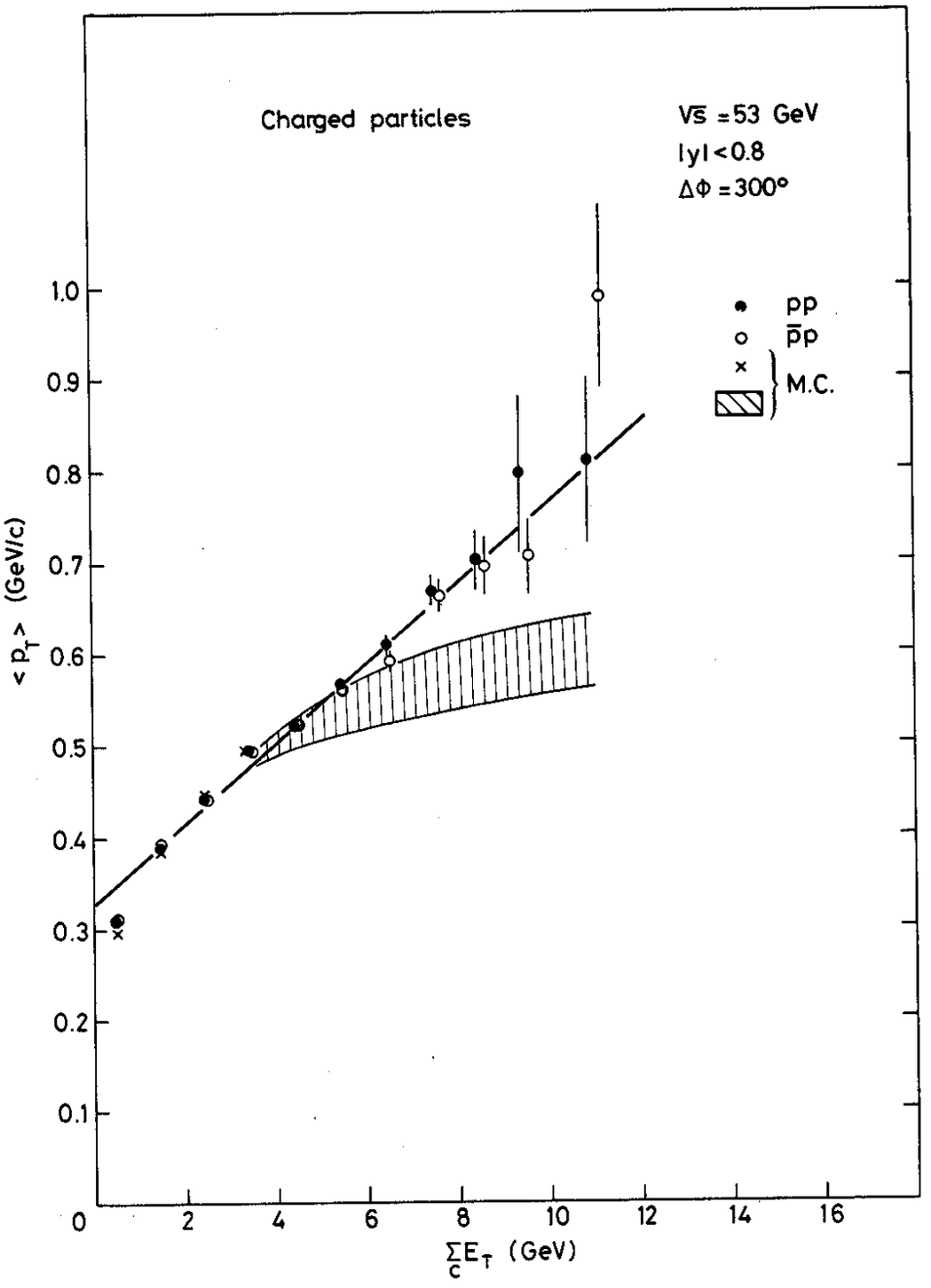
Charged particles
√s = 53 GeV
|y| < 0.8
Δφ = 300°
pp
p̄p
M.C.
< p_T > (GeV/c)
Σ_c E_T (GeV)
0
0.1
0.2
0.3
0.4
0.5
0.6
0.7
0.8
0.9
1.0
2
4
6
8
10
12
14
16

Fig. 7 a)

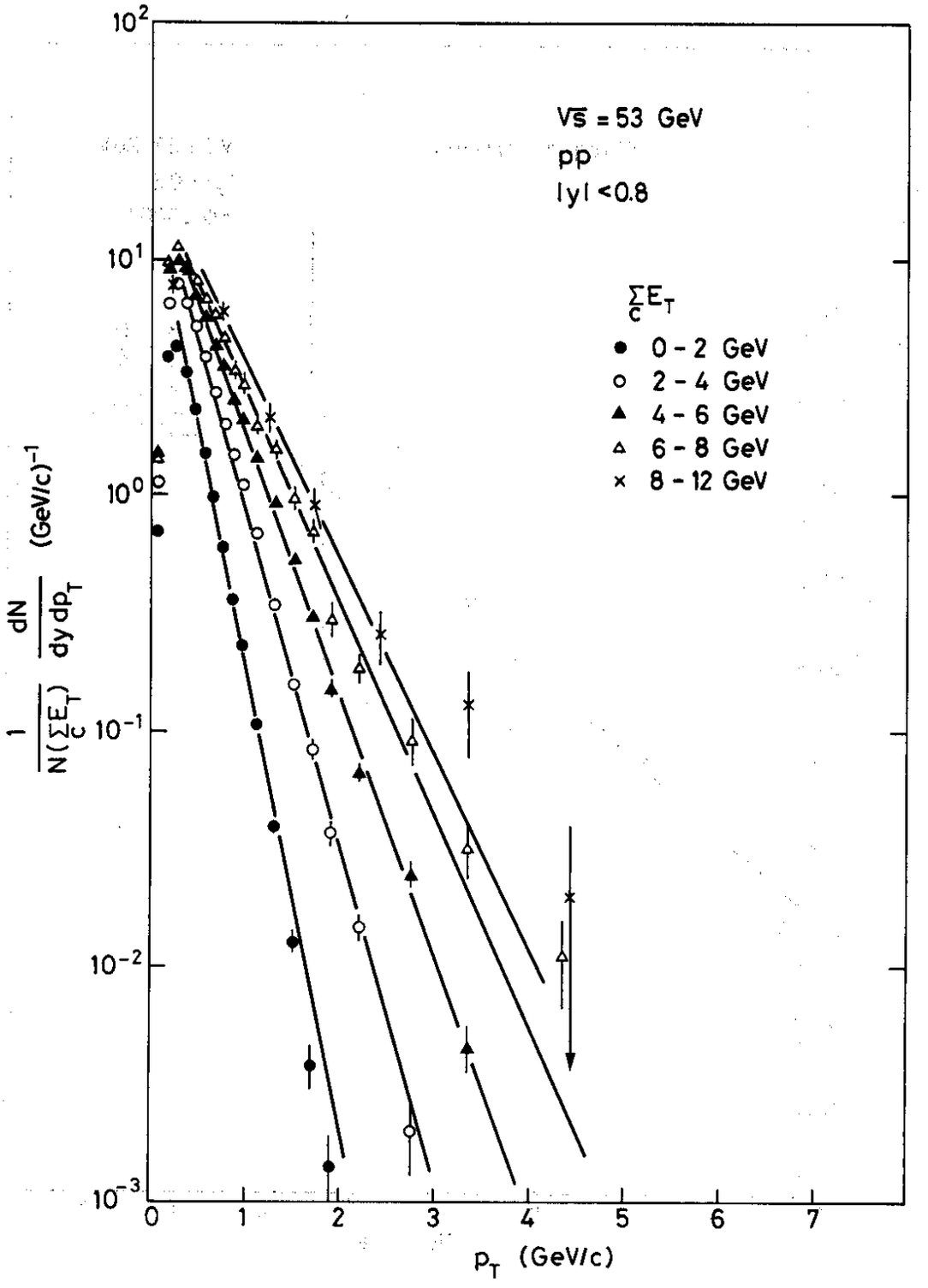
10^2
10^1
10^0
10^{-1}
10^{-2}
10^{-3}
$\sqrt{s}$ = 53 GeV
pp
|y| <0.8
$\sum_c E_T$
0 - 2 GeV
2 - 4 GeV
4 - 6 GeV
6 - 8 GeV
8 - 12 GeV
$\frac{1}{N(\sum_c E_T)} \frac{dN}{dy\, dp_T}$ (GeV/c)$^{-1}$
0
1
2
3
4
5
6
7
p_T (GeV/c)

Fig. 7 b)

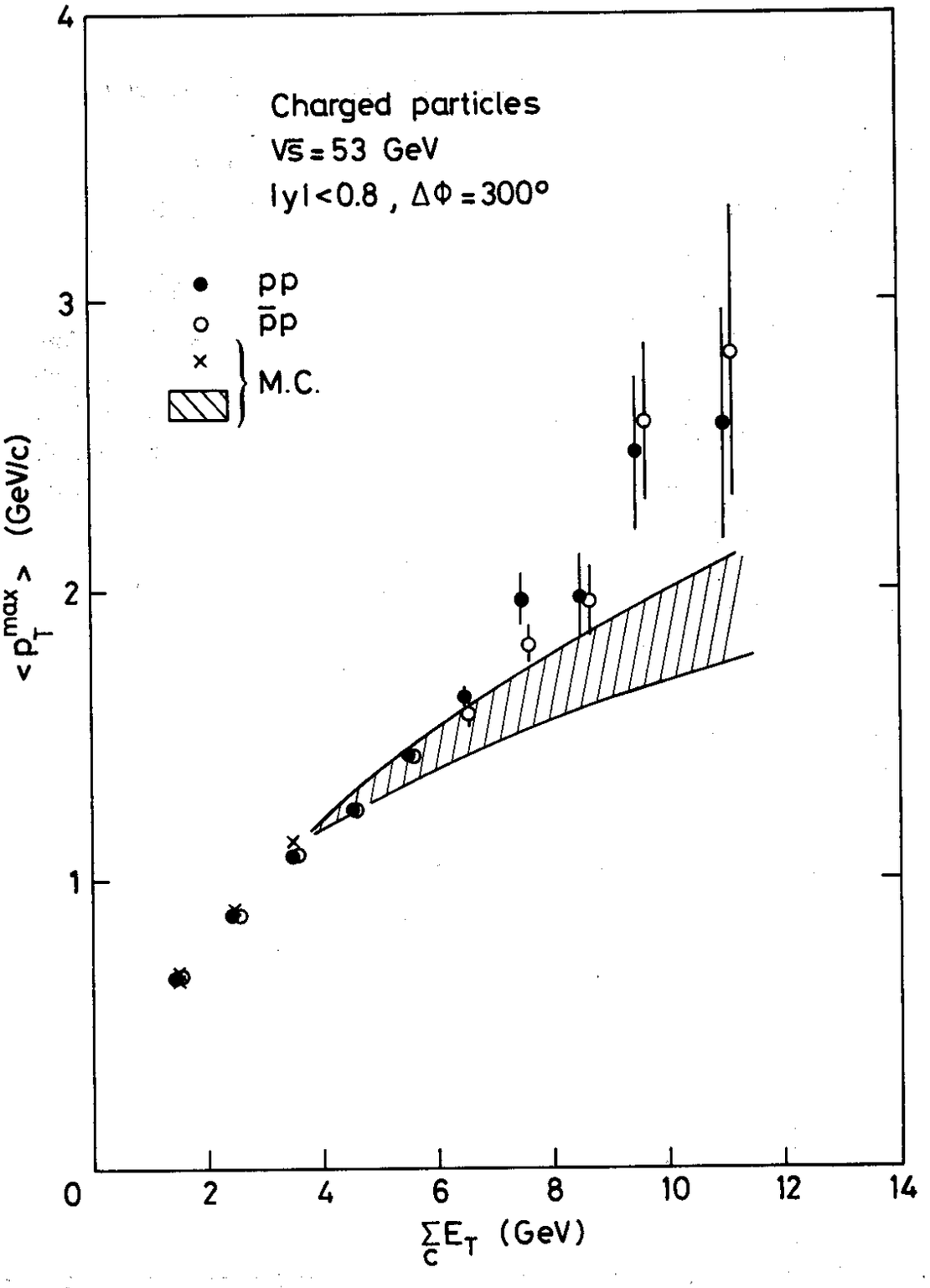
Charged particles
√s = 53 GeV
|y| < 0.8 , Δφ = 300°
pp
p̄p
M.C.
< p_T^max > (GeV/c)
Σ_C E_T (GeV)
0
1
2
3
4
2
4
6
8
10
12
14

Fig. 8 a)

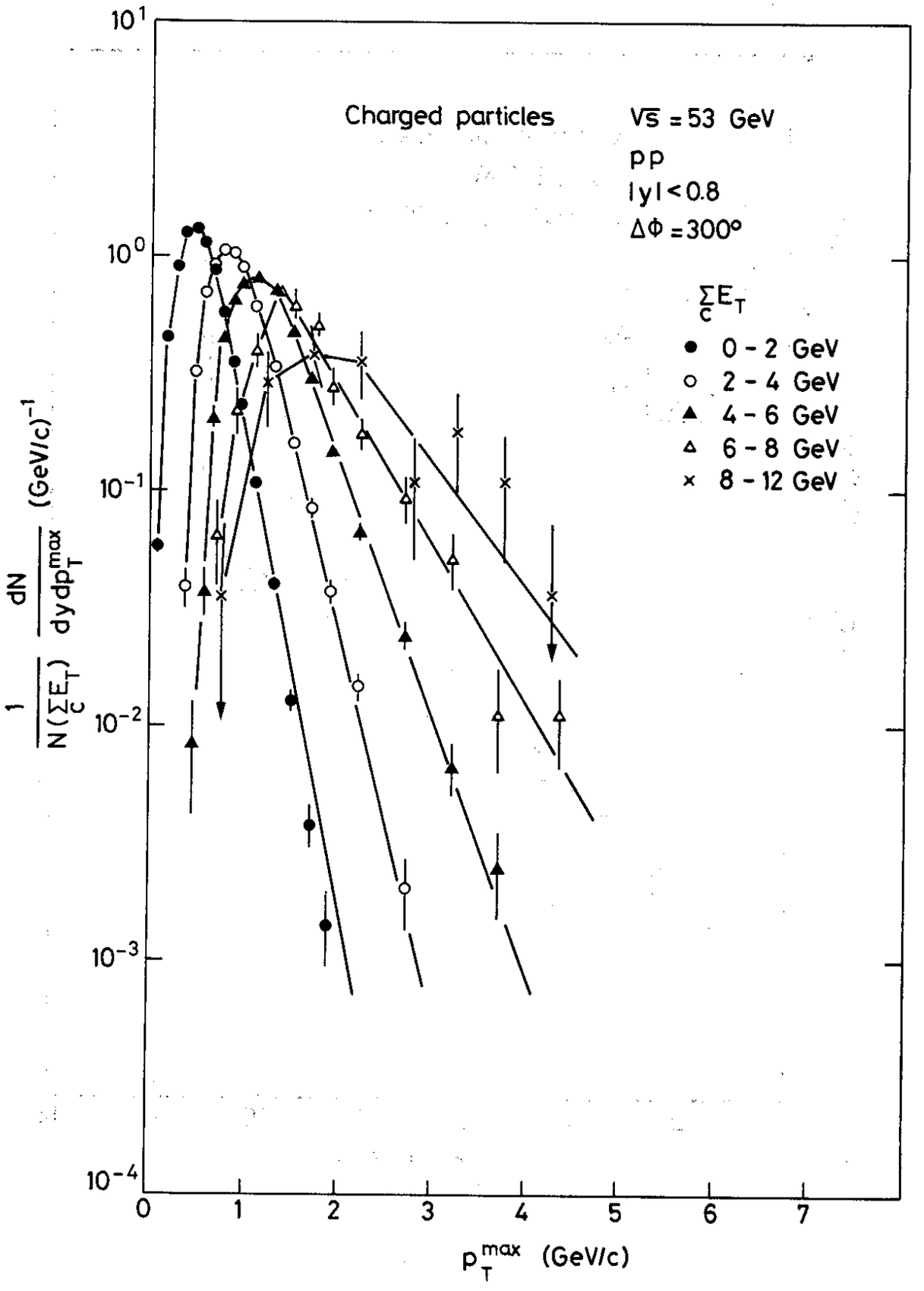
Charged particles
√s = 53 GeV
pp
|y| < 0.8
Δφ = 300°
Σ E_T
0 - 2 GeV
2 - 4 GeV
4 - 6 GeV
6 - 8 GeV
8 - 12 GeV
1/N(Σ E_T) dN/dy dp_T^max (GeV/c)^-1
p_T^max (GeV/c)

Fig. 8 b)

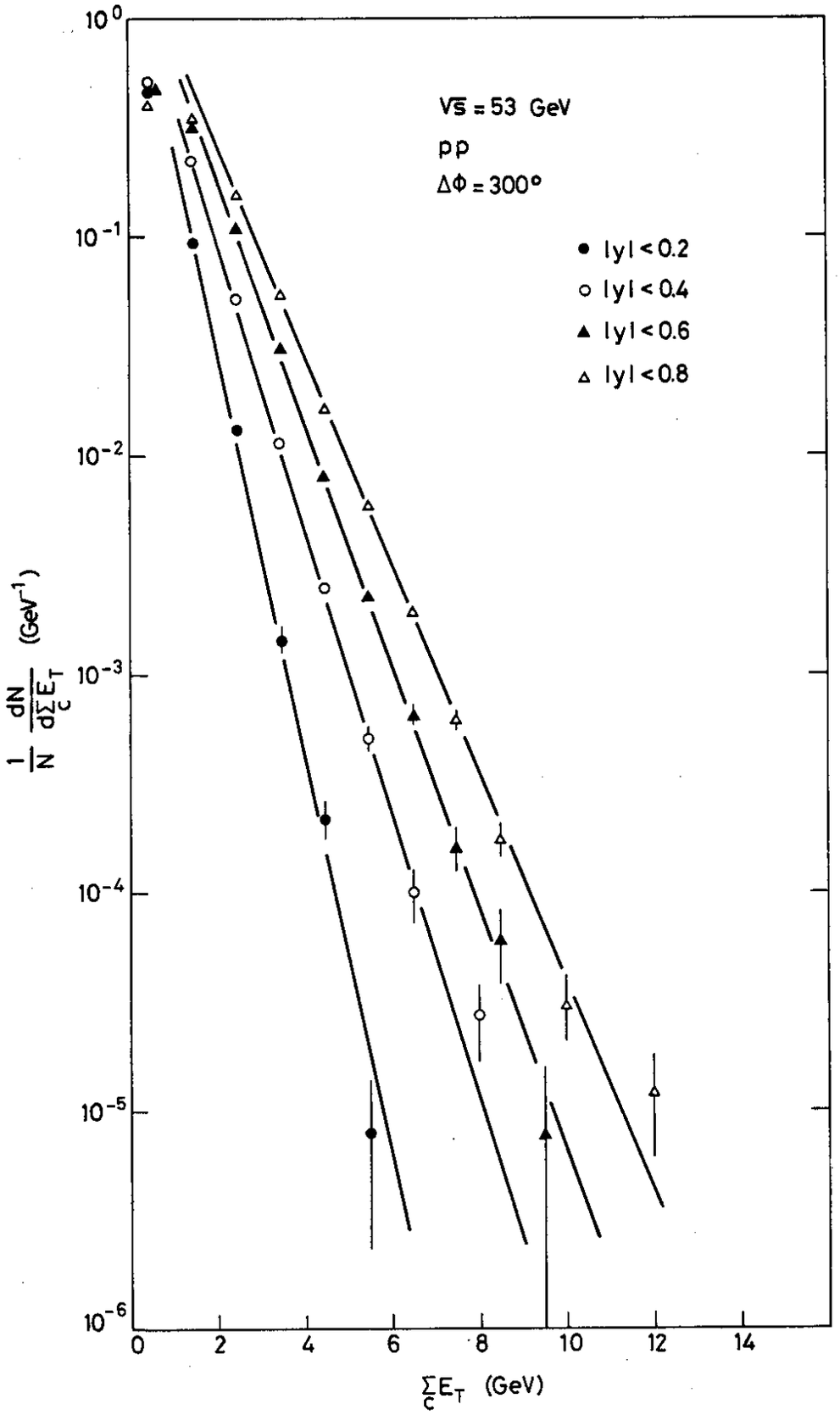
10^0
10^{-1}
10^{-2}
10^{-3}
10^{-4}
10^{-5}
10^{-6}
$\sqrt{s}$ = 53 GeV
pp
$\Delta\Phi$ = 300°
● |y| < 0.2
○ |y| < 0.4
▲ |y| < 0.6
△ |y| < 0.8
$\frac{1}{N}\frac{dN}{d\sum_c E_T}$ (GeV^{-1})
0
2
4
6
8
10
12
14
$\sum_c E_T$ (GeV)

Fig. 9 a)

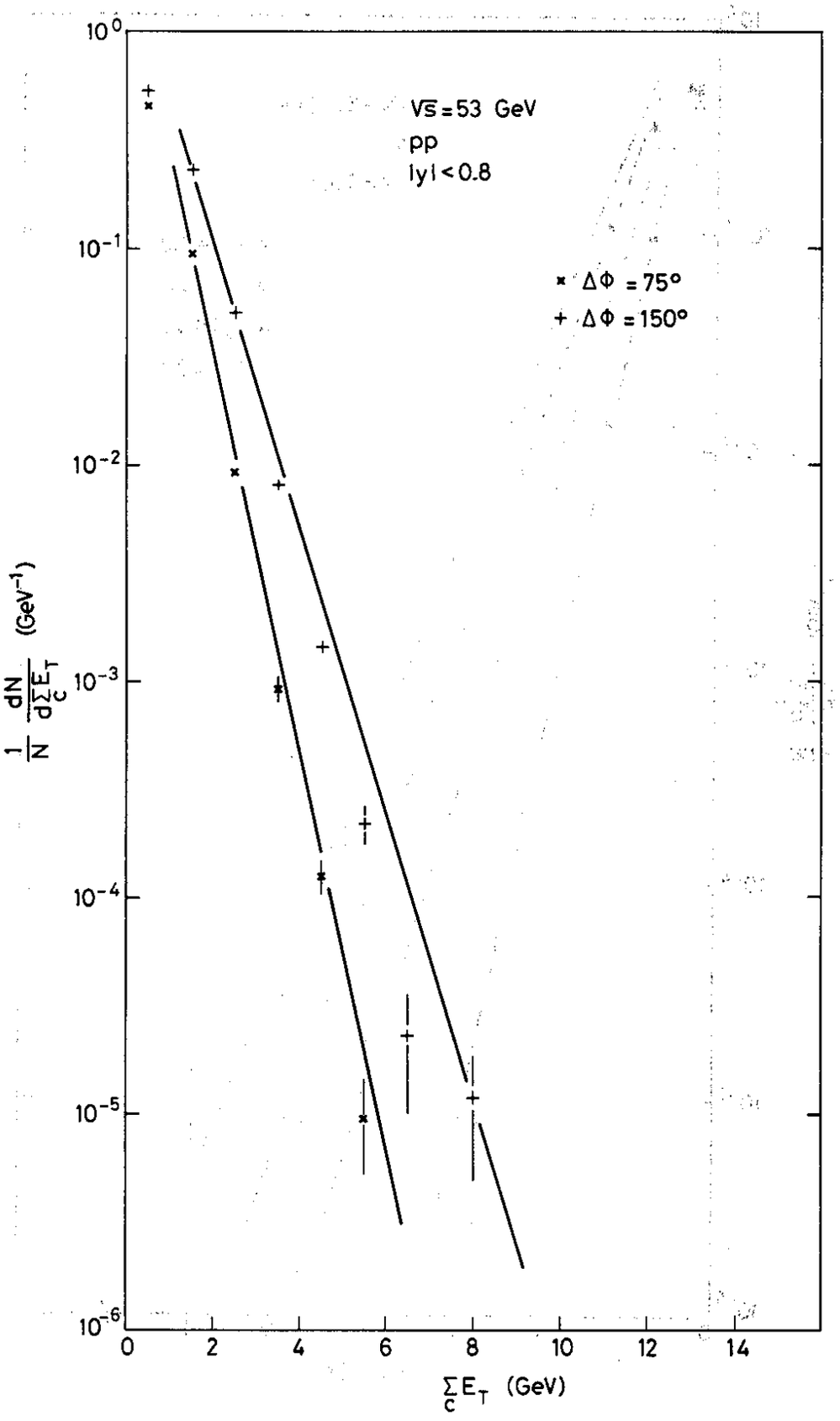
10^0
10^{-1}
10^{-2}
10^{-3}
10^{-4}
10^{-5}
10^{-6}
$\frac{1}{N}\frac{dN}{d\sum_c E_T}$ (GeV^{-1})
$\sqrt{s}$ = 53 GeV
pp
|y| < 0.8
× Δφ = 75°
+ Δφ = 150°
0
2
4
6
8
10
12
14
$\sum_c E_T$ (GeV)

Fig. 9 b)

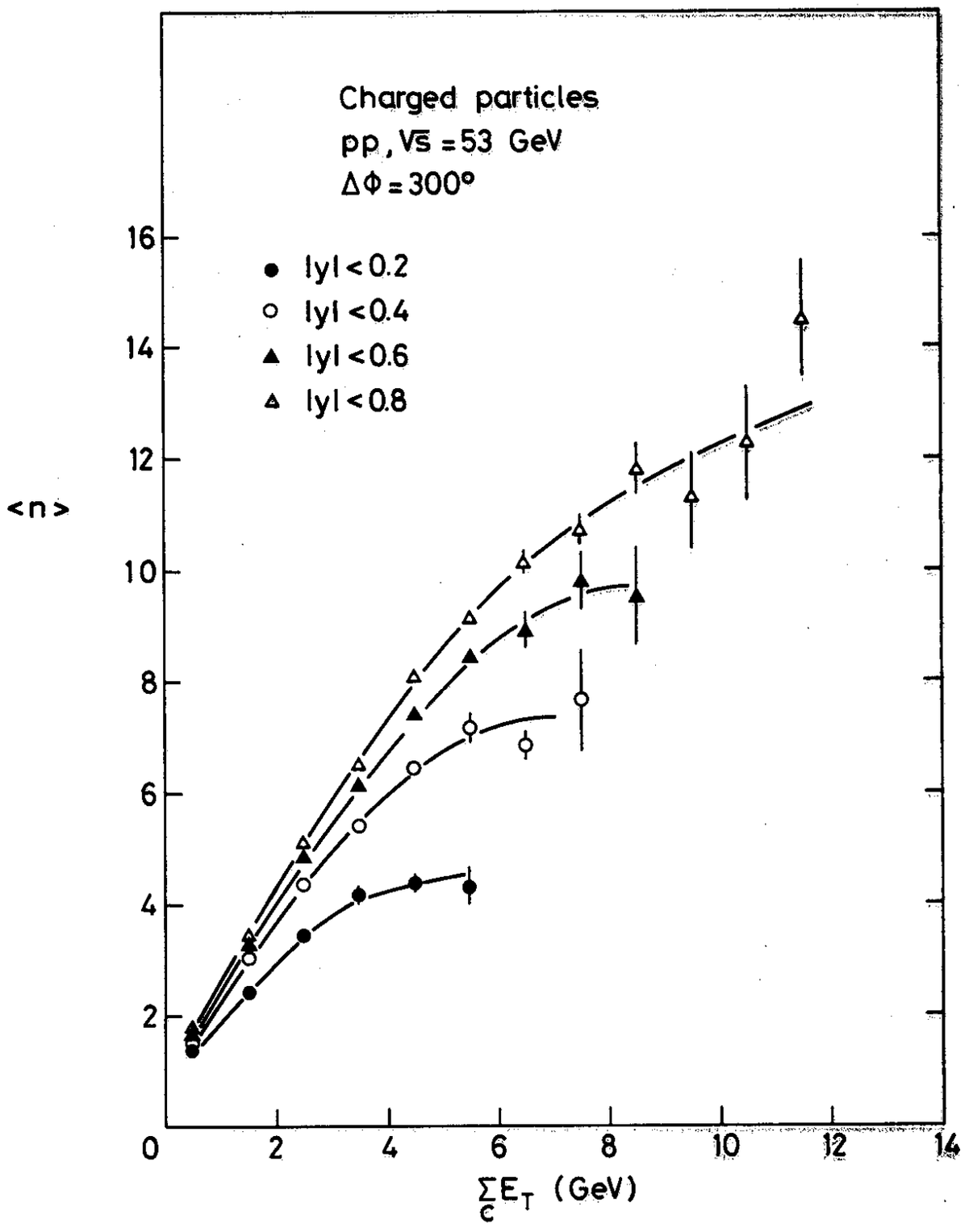
Charged particles
pp, √s = 53 GeV
Δφ = 300°
● |y| < 0.2
○ |y| < 0.4
▲ |y| < 0.6
△ |y| < 0.8
<n>
0
2
4
6
8
10
12
14
16
Σ E_T (GeV)
c

Fig. 10

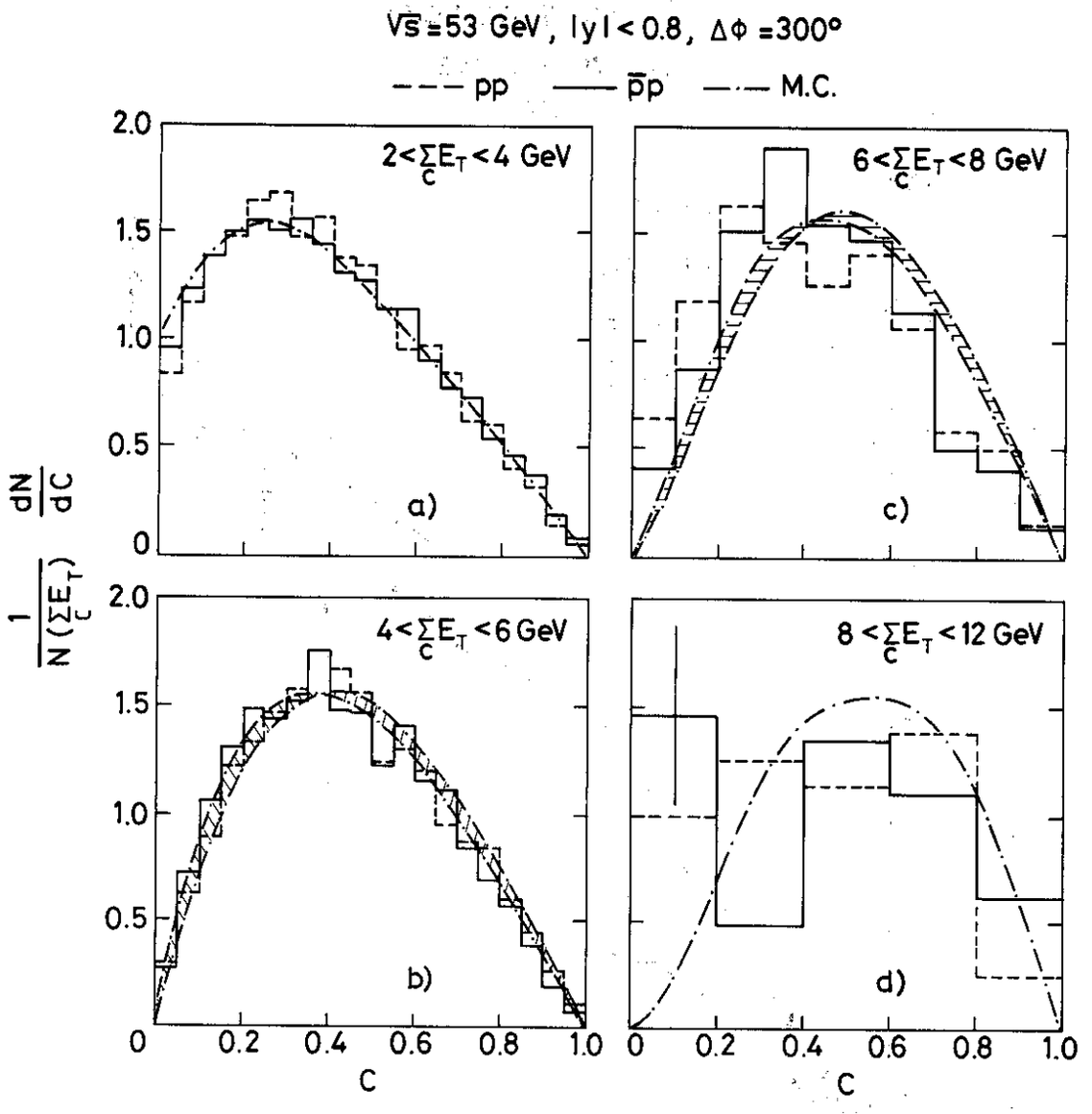
√s = 53 GeV, |y| < 0.8, Δφ = 300°
--- pp —— p̄p —·— M.C.
2<ΣE_T<4 GeV
6<ΣE_T<8 GeV
4<ΣE_T<6 GeV
8<ΣE_T<12 GeV
a)
b)
c)
d)
dN/dC
1/N(ΣE_T)
C
C
0
0.5
1.0
1.5
2.0
0.2
0.4
0.6
0.8

Fig. 11

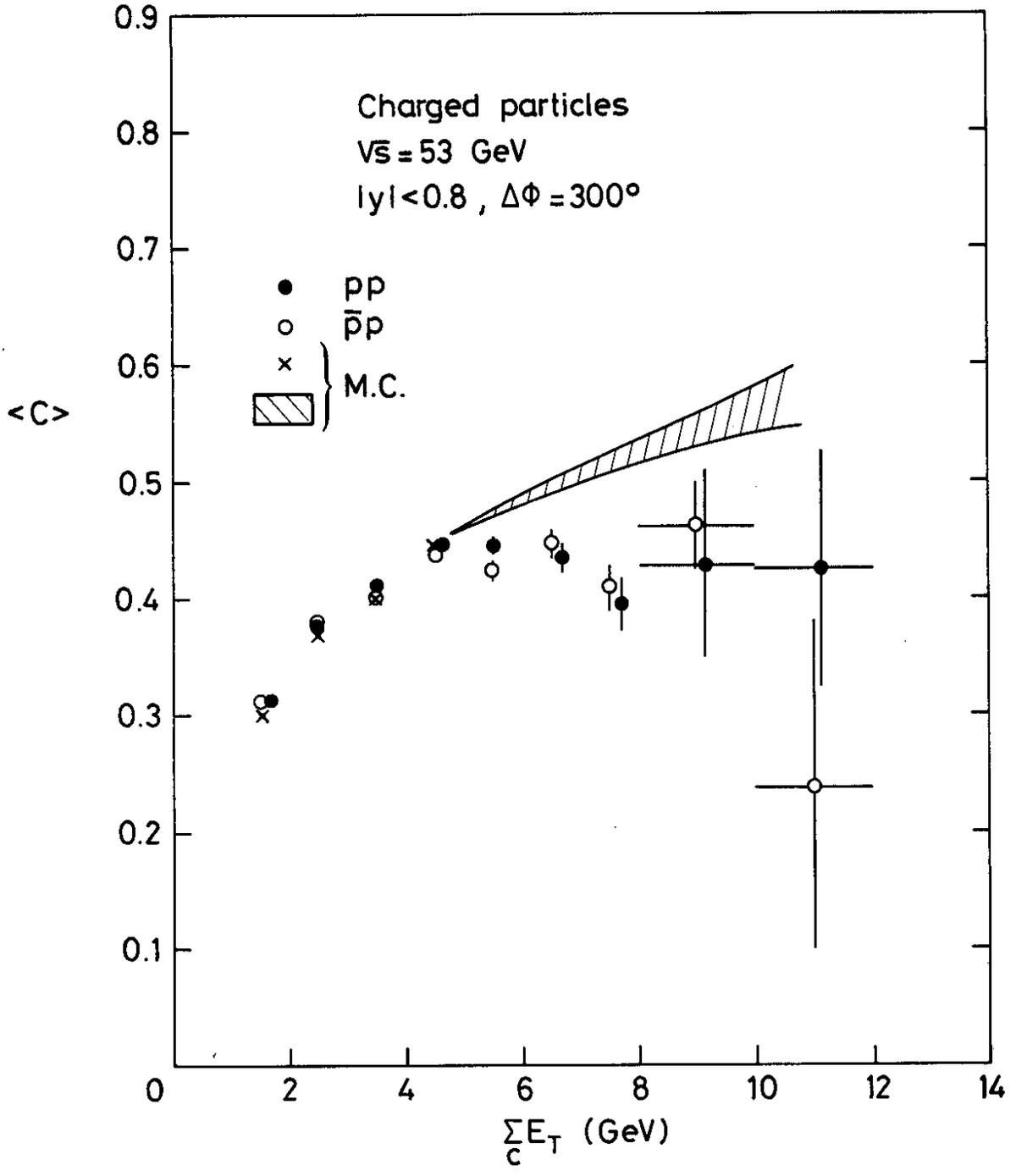
Charged particles
√s = 53 GeV
|y| < 0.8 , Δφ = 300°
pp
p̄p
M.C.
<C>
0.9
0.8
0.7
0.6
0.5
0.4
0.3
0.2
0.1
0
2
4
6
8
10
12
14
Σ E_T (GeV)
c

Fig. 12